Materials Today Bio 26 (2024) 101109

Contents lists available at ScienceDirect

Materials Today Bio

journal homepage: www.journals.elsevier.com/materials-today-bio

Nanofiber-microwell cell culture system for spatially patterned differentiation of pluripotent stem cells in 3D

Youyi Tai [a], Robyn Goodrich [a], Maricela Maldonado [b], Jessica Ortiz [a], Jeniree Martinez [a], Gerardo Ico [a], Angel Ko [a], Hung Ping Shih [c], Jin Nam [a,*]

[a] Department of Bioengineering, University of California, Riverside, CA, 92521, USA
[b] Department of Biomedical Engineering, California State University Long Beach, CA, 90840, USA
[c] Department of Translational Research and Cellular Therapeutics, City of Hope, CA, 91010, USA

ARTICLE INFO

Keywords:
Electrospun nanofibers
Microfabrication
Pluripotent stem cell differentiation
Mechanobiology

ABSTRACT

The intricate interplay between biochemical and physical cues dictates pluripotent stem cell (PSC) differentiation to form various tissues. While biochemical modulation has been extensively studied, the role of biophysical microenvironments in early lineage commitment remains elusive. Here, we introduce a novel 3D cell culture system combining electrospun nanofibers with microfabricated polydimethylsiloxane (PDMS) patterns. This system enables the controlled formation of semispherical human induced pluripotent stem cell (hiPSC) colonies, facilitating the investigation of local mechanical stem cell niches on mechano-responsive signaling and lineage specification. Our system unveiled spatially organized RhoA activity coupled with actin-myosin cable formation, suggesting mechano-dependent hiPSC behaviors. Nodal network analysis of RNA-seq data revealed RhoA downstream regulation of YAP signaling, DNA histone modifications, and patterned germ layer specification. Notably, altering colony morphology through controlled PDMS microwell shaping effectively modulated the spatial distribution of mechano-sensitive mediators and subsequent differentiation. This study provides a cell culture platform to decipher the role of biophysical cues in early embryogenesis, offering valuable insights for material design in tissue engineering and regenerative medicine applications.

1. Introduction

Stem cells not only possess significant therapeutic potential for tissue engineering and cell therapy applications but also provide an opportunity to develop disease and/or patient-specific in vitro models as drug testbeds or for pathological studies. Embryonic stem cells (ESCs) and induced pluripotent stem cells (iPSCs), collectively known as pluripotent stem cells (PSCs), have been extensively investigated due to their unlimited self-renewal and potent differentiation capability towards phenotypes in all three germ layer lineages [1,2]. To develop tissue replacements or in vitro models for various developmental, pathological, and pharmaceutical studies, carefully formulated biochemical factors, typically gained from developmental biology studies, have been well explored to guide the differentiation of stem cells towards specific tissues/cells with unique functionality [3–6].

Beyond biochemical cues, the intricate interplay of mechanical forces, also known as mechanotransductive signals, significantly shapes stem cell fate and behavior during development, influencing morphological organization and differentiation [7,8]. Recognizing this, researchers have harnessed diverse materials, systems, and techniques to design in vitro models replicating unique physical microenvironments and their impact on pluripotent stem cell (PSC) behavior. For instance, studies have employed cell adhesive ligand patterns or molding approaches to induce the formation of 2D PSC colonies exhibiting defined morphologies and differentiation patterns [9–12]. Such patterned differentiation likely arises from the interplay of physical microenvironment-mediated cell-matrix interactions and cell-cell communication [9,11]. While these 2D iPSC in vitro models have unveiled intriguing insights into patterned PSC differentiation, their inherent limitation lies in the two-dimensionality, failing to capture the intricate 3D cell-cell interactions occurring in vivo. Notably, variations in 3D cell-cell interactions have been shown to elicit diverse cellular responses, potentially leading to ambiguous or even contradictory results in PSC differentiation studies [13]. Therefore, to more faithfully mimic human in vivo development and achieve consistent PSC differentiation patterns, there is a crucial need for novel in vitro models

* Corresponding author.
E-mail address: jnam@engr.ucr.edu (J. Nam).

https://doi.org/10.1016/j.mtbio.2024.101109
Received 5 February 2024; Received in revised form 4 May 2024; Accepted 31 May 2024
Available online 1 June 2024

capable of inducing the formation of well-defined 3D PSC colonies.

In this regard, we engineered a robust and tunable stem cell culture platform, composed of electrospun polycaprolactone (PCL) nanofibers and microfabricated polydimethylsiloxane (PDMS) microwells (nanofiber-microwell cell culture system), to provide the physical/mechanical support for iPSCs to develop 3D hemispherical colonies, where individual cells within the colony experience heterogeneous mechanical forces in a residing location-dependent manner. By optimizing the sizes of microwells on PCL nanofibrous substrates, which were tuned to enable the 3D stem cell colony formation in our previous study [3,14], a spatially patterned germ layer differentiation was developed within the colonies. In addition, we found that the differentiation of the cells in these colonies is significantly affected by the mechanotransduction pathway, including the mechano-sensing regulator, rho-associated protein kinase (RhoA/ROCK), and the downstream effector, yes-associated protein (YAP). A close interaction between the mechano-sensing and DNA histone modification was revealed, potentially demonstrating the important role of epigenetic regulation in mediating physical environment-induced spatially patterned differentiation. Such spatially organized physical environment within the 3D iPSC colony and its effect on subsequent germ layer differentiation was further confirmed by altering the form of the 3D colonies through the shape alteration of the microwells. Overall, the nanofiber-microwell cell culture system provides a robust platform for developing an in vitro 3D iPSC differentiation model to gain insight into mechanotransduction signaling and its effect on cellular behaviors.

2. Materials and methods

2.1. Synthesis of PCL nanofibrous substrate

Electrospun PCL nanofibrous substrates were synthesized as previously described [14]. Briefly, a precursor solution of 8.5 wt% PCL (M.W. 80 k, Sigma Aldrich) dissolved in 5:1 trifluoroethanol (Sigma Aldrich)-water was electrospun using a custom electrospinning setup [14]. The electrospinning parameters for the substrate synthesis have been optimized to achieve approximately 500 nm average fiber diameter with a reduced Young's modulus of 19 kPa [14].

2.2. Microfabrication of PDMS mold

Standard photolithography-based microfabrication method was used to produce patterned silicon wafers, involving a series of oxidation, photolithography, and etching steps. Briefly, a 3 μm thick silicon dioxide (SiO_2) layer was coated on as-received silicon (Si) wafers, via plasma-enhanced chemical vapor deposition using a Plasmatherm 790 (Plasma-Therm). A positive photoresist (PR) was spin-coated and exposed to the UV light through a patterned mask having the required dimensions of the microwells. The PR was developed yielding the micropatterning of the wells on top of the SiO_2 layer. The SiO_2 layer, which was not protected by the PR layer, was then etched using the Surface Technology Systems Reactive Ion Etcher. The PR was used as an etching buffer layer so that we could etch past the 3 μm SiO_2 layer that is immediately exposed to the ion etching and into the Si without compromising the micropillars, which act as the master mold. The patterned Si wafer was then washed in acetone, isopropanol, and DI water to remove and clean the remaining PR. The resulting Si/SiO_2 wafer was then placed in diluted hydrofluoric acid to remove the SiO_2 from the micropillars, revealing the master mold having various diameters of micropillars for further processing.

To fabricate the PDMS-based microwells, a photoresist (SU-8) was spin-coated on the Si master mold at low spin speeds to avoid comet tailing around the micropillars of the master mold. The SU-8 was soft-baked at 65 °C for 10 min on a hotplate. Once cooled, PDMS (Sylgard 184 Silicone) was spin-coated at 800 rpm to promote even distribution. The PDMS on the master mold was then cured at 65 °C for 4 h. Once cured, the PDMS was lifted off by placing the assembly in a bath of acetone with gentle agitation. The PDMS reverse mold was detached from the master mold and cut into appropriate sizes. In order to make the stretched PDMS molds with an ellipsoidal microwell shape, the curing time was reduced to 2 h allowing for the formation of half-cured PDMS films. These films were then mechanically stretched at 60 °C for 12 h to transform circular wells into elliptical hollows with an aspect ratio of 2.5:1 using a tensile force generator. This aspect ratio was achieved by using a stretching ratio of 3:1 to compensate for the spring back of the viscoelastic PDMS mold. PolyHEMA was applied to the surface of both circular and stretched PDMS molds to increase the hydrophobicity of the PDMS surface, preventing direct cell attachment outside of the microwells. The coated PDMS molds were stored at 4 °C before being assembled with electrospun nanofibrous PCL substrates, which were subjected to air plasma treatment prior to assembly. The PDMS molds were heated at 55 °C, then heat pressed onto the PCL substrates to glue them together. The assembled nanofiber microwells (8 mm in diameter) were placed in a 24-well culture plate and X-ray irradiated for sterilization.

2.3. Cell culture

A well-characterized human iPSC line and a human embryonic stem cell line (H9-ESC, WAe009-A) were used in this study [14]. Cells were maintained on Geltrex®-coated (Life Technologies) tissue culture plates in mTeSR1 growth media (StemCell Technologies) and seeded onto the nanofiber-microwell substrates at a cell density of approximately 120,000 cells per cm^2. A ROCK inhibitor, Y-27632 (10 μM, Sigma Aldrich), was supplemented into the media to improve initial cell attachment and survival. The following day, Y-27632 was removed from the media unless otherwise noted.

To examine the simultaneous multi-lineage differentiation behavior of iPSCs within individual 3D colonies, iPSCs were pre-cultured for 5 days and then treated with BMP4 (40 ng mL^{-1}) for 36 h. Differentiated 3D iPSC colonies were fixed using 4 % paraformaldehyde.

To examine if RhoA/ROCK or YAP regulates spatially patterned germ layer differentiation of 3D iPSC colonies, iPSCs were pre-cultured for 5 days and subsequently treated with BMP4 (40 ng mL^{-}) for 36 h. ROCK activator (calpeptin, 30 μM, Sigma) or YAP activator (PY60, 16 μM, Sigma) was added into the cell culture media for 38 h (2 h during the preculture duration+36 h of differentiation duration). Cells were then fixed using 4 % paraformaldehyde.

To examine the relationship between YAP and DNA histone modifications, iPSCs were pre-cultured for 5 days and subsequently treated with YAP inhibitor (verteporfin, 5 μM, Tocris) for 2 h at the end of the 5-day pre-culture period. Cells were then fixed using 4 % paraformaldehyde.

For the analysis of colony-morphology-dependent cellular behaviors, iPSC colonies with an elliptical-dome shape were formed using an elongated microwell as described above. Subsequently, colonies were either fixed using 4 % paraformaldehyde or treated with BMP4 for 36 h before the fixation.

2.4. RNA sequencing

To assess the differences in the epigenetic regulations between 2D iPSC colonies and 3D iPSC colonies, total RNA from the iPSCs grown in either 2D or 3D form was isolated using the RNeasy Micro Kit (Qiagen) according to the manufacturer's instructions. cDNA libraries were then prepared using the KAPA RNA Hyperprep Kit with RiboErase (HMR). The established libraries were subjected to sequencing on Illumina HiSeq 2500 (50 bp, single-ended). For sequence alignment and gene counts, RNA-seq reads were trimmed to remove sequencing adapters using Trimmomatic and polyA tails using FASTP [15,16]. The processed reads were mapped back to the human genome using STAR software [17]. The normalization of gene expression fold change was conducted

using RSeQC software. Among the whole gene set with the normalized expression values, epigenetic-related genes consisting of m6A-related genes, histone modification-related genes, RNA binding proteins, transcription factors, and DNA methylases were collected based on previous literature and databases [18]. A hierarchical clustering was performed to reveal the differences in epigenetic-related gene expression between the Control and the 3D colony cells using Cluster and Treeview software. GSEA software, which used a list of whole epigenetic-related gene sets with the normalized fold change value, was further used to conduct GO analysis and subsequent epigenetic-related biological process enrichment evaluation [19,20]. The number of permutations for p-value calculation was set to 1000 and the top 5 enriched epigenetic-related biological processes, with the criteria of a p value < 0.05, were selected and plotted using the Origin software. A heatmap was plotted indicating the methylation- and acetylation-related gene expressions. In addition, the overall gene sets enriched in the GSEA were organized into a graphical network produced using "Enrichment Map" plugins in Cytoscape; each node in the network map represents an enriched gene set of a specific biological process. Three different clusters (annotated automatically by the AutoAnnotate plugin) were chosen to reveal potential interactions among them. The RNA sequencing data are available at Gene Expression Omnibus (GSE234529).

2.5. Immunofluorescence imaging

The fixed samples were stained following a standard immunofluorescence staining protocol with modifications to improve the antibody diffusion throughout the entire colony. The fixed colonies were permeabilized in concentration-optimized chemical detergent (Triton X-100) with mechanical shaking, followed by background suppression using 1 % bovine serum albumin [21]. The following antibodies with experimentally determined optimal concentrations were utilized for immunostaining: mouse anti-NANOG (Abcam), goat anti-BRACHYURY (R&D Systems), mouse anti-PAX6 (Developmental Studies Hybridoma Bank (DSHB)), mouse anti-active RhoA (NewEast Bioscience), mouse anti-α-tubulin (DSHB), mouse anti-Non Muscle Myosin Light Chain (DSHB), rabbit anti-SOX2 (Cell Signaling), rabbit anti-SOX17 (Proteintech), rabbit anti-SOX1 (Proteintech), rabbit anti-H3K4me3 (Abcam), rabbit anti-H3K27ac (Abcam), rabbit anti-H3K27me3 (Abcam), rabbit anti-H3K9me3 (Abcam), rabbit anti-YAP-488 (Cell Signaling). Except for the YAP antibody, which was pre-conjugated with Alexa Fluor 488, the corresponding secondary antibodies were used appropriately: Alexa Fluor 488 donkey anti-mouse IgG (H + L), Alexa Fluor 488 goat anti-rabbit IgG (H + L), Alexa Fluor 594 goat anti-mouse IgG (H + L), or Alexa Fluor 488 donkey anti-goat IgG (H + L) (Invitrogen). The samples were then counter-stained, if necessary, using phalloidin (Abcam) and DAPI (Sigma) to visualize actin and nuclei. The tissue clearing process (50 % formamide with 20 % polyethylene glycol) was employed after the staining for improved visualization under the volume confocal scanning and imaging (Zeiss 800) [22].

2.6. Confocal image quantification

Confocal images were quantified to further investigate the spatial distribution of various markers within iPSC colonies. Briefly, the radius of the sphere, which overlaps the contour of the semi-spherical iPSC colony, determined from DAPI staining, was first calculated based on the Pythagorean theorem (Fig. S1A). For each confocal section, positively stained cells with a marker of interest were located and the distance from each cell to the center of the section was calculated (Fig. S1B). The distance to the sphere center was then calculated (Fig. S1C). All the results from multiple sections were collected for each marker and histograms were generated (Fig. S1D). The ratio of positively stained cells with a marker of interest to the DAPI-stained cells was finally calculated with respect to the normalized distance to the center of the sphere.

2.7. Statistical analysis

All experiments were conducted with a minimum of triplicate biological samples and data are represented as mean ± standard deviation (SD). Comparison of groups for statistical significance was determined using SPSS 115 software with either one-way ANOVA with Tukey's HSD post-hoc or one sample student T-test. Statistical significance was reported when a 'p' value was less than 0.05. Pearson's correlation coefficient (r) was determined to reveal the bivariate correlation between two factors. $r > 0.5$ indicates a strong positive correlation, $0 < r < 0.5$ indicates a moderate or weak positive correlation, and $r < 0$ indicates a negative correlation [23,24].

3. Results

3.1. Nanofiber-microwell cell culture system is optimized to induce the formation of 3D iPSC colonies

We have previously shown that the use of a soft electrospun substrate enabled the observation of mechano-responsive 3D colony formation [14]. In order to maintain the structure of such 3D iPSC colonies during the differentiation process, we designed a cell culture system by combining the electrospun PCL nanofibrous substrate with a PDMS mold, having microwells with various diameters, to physically restrict the size and morphology of iPSC colonies. The fabrication of the microwell cell culture system involves the standard process of photolithography-based microfabrication, deep etching, PDMS casting, and PCL substrate-PDMS mold assembling (Fig. 1A). The patterned silicon wafer (Fig. 1B), which was fabricated by deep etching, was used as a negative to form a PDMS mold (150 μm thickness) having patterned microwells (Fig. 1C). Electrospun nanofibrous PCL substrate was then attached to the PDMS mold with its fibrous morphology exposed only in those patterned wells (Fig. 1D and E). The hydrophobic treatment of the PDMS mold with polyHEMA inhibits the adhesion of iPSCs on the PDMS surfaces, enabling iPSCs to grow and form 3D colonies only on the exposed PCL nanofibers within the microwells (Fig. 1F). To determine the optimal microwell size, iPSCs were cultured in the cell culture system having various microwell diameters (Fig. 1G–I). The most uniform and consistent morphology of iPSC colonies was observed in microwells having 200 μm diameter, as compared to the cells that were cultured in 150 μm or 250 μm sized microwells. Therefore, the 200 μm microwell diameter was used in the subsequent experiments.

3.2. 3D iPSC colonies in the nanofiber-microwell cell culture system exhibit a spatially patterned cytoskeletal organization and subsequent germ layer differentiation

Since RhoA and cytoskeletal structure actively respond to the change in the surrounding microenvironment [25–27], their heterogeneous expression within the 3D iPSC colonies induced by the nanofiber-microwell cell culture system was examined. Interestingly, RhoA activation was confined to the outermost layers of the 3D colony (Fig. 2A, Fig. S2A), potentially indicating the spatial heterogeneity in the mechanical environment within a 3D colony. As the RhoA/ROCK signaling often affects the downstream cytoskeleton organization [28,29], the expression patterns of α-tubulin, actin, and non-muscle myosin light chain (MLC) were analyzed. Similar to the active RhoA expression pattern, α-tubulin was highly localized at the outermost layers of the colony (Fig. 2B, Fig. S2B), likely indicating the generation of greater tension at the outermost layer in the spherical colony. This coinciding radial expression pattern between active RhoA and α-tubulin suggests the regulation of cytoskeletal components by the RhoA/ROCK signaling. The expression of MLC exhibited a more uniform distribution throughout the entire 3D iPSC colony as compared to the expression of α-tubulin (Fig. 2C, Fig. S2C). The colocalization between MLC and actin especially at the outermost layers of the colony (Fig. 2C, magnified

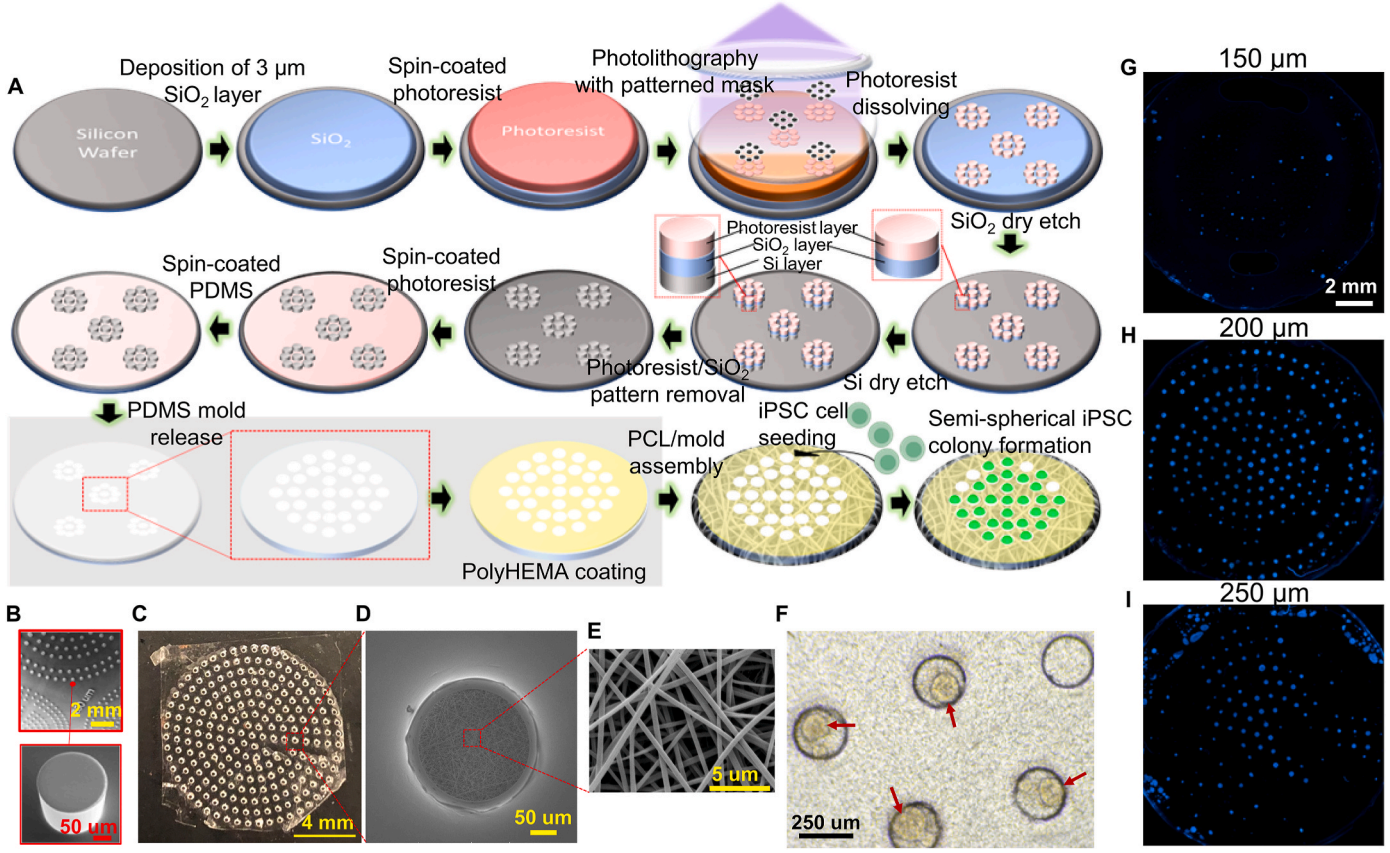

Fig. 1. Nanofiber-microwell cell culture system is optimized to induce the formation of 3D iPSC colonies. (A) A schematic shows the fabrication process of the nanofiber-microwell cell culture system. (B–F) Representative images of a (B) patterned silicon wafer, (C) PDMS microwell mold, (D) PCL electrospun substrate-PDMS mold assembly, (E) nanofibrous PCL in the bottom of a microwell, and (F) cell colony growth within microwells. Red arrows indicate the cell colonies. (G–I) Representative fluorescent DAPI images showing the distribution of iPSC cell colonies in the nanofiber-microwell cell culture systems with different sizes of microwells. (For interpretation of the references to color in this figure legend, the reader is referred to the Web version of this article.)

bottom), however, suggests actin-myosin interactions, likely induced by the RhoA/ROCK-mediated MLC phosphorylation [30–32]. This interaction often results in the formation of actomyosin cable, stabilizing the colony structure and affecting differentiation [33,34]. It should be noted that a uniform expression of active RhoA was observed in 2D monolayer iPSC colonies, as compared to the spatially patterned expression of RhoA within 3D iPSC colonies (Fig. S2D).

To investigate if this spatially patterned mechanical microenvironment would affect the differentiation of iPSCs, 3D iPSC colonies were subjected to BMP4 stimulation for 36 h to induce simultaneous multilineage differentiation [12,35]. Hereinafter, the cells pre-cultured in the microwell cell culture system for 5 days to form 3D colonies are noted as the pre-differentiation condition (Prediff) while those subsequently subjected to BMP4 treatment after the pre-culture are noted as the differentiation condition (Diff). Under the Diff condition, a unique pattern of spatially organized differentiation was observed where T and SOX2 expression was radially arranged from the edge to the center of the 3D iPSC colony (Fig. 2D, Fig. S3A). The expression of endodermal SOX17 colocalized with T expression (Pearson's correlation coefficient of 0.922), suggesting the very early stage of mesendodermal differentiation [36] (Fig. 2E, Fig. S3B). This spatially organized differentiation pattern in 3D iPSC colonies is clearly notable in the location tracking analysis, where $SOX2^+$ cells were positioned in the inner parts of the colony while T^+ and $SOX17^+$ cells were localized at the outermost layers (Fig. 2F and G). Since SOX2 is also a pluripotency marker, the absence of NANOG expression and the presence of SOX1 expression were used to confirm the early stage of ectodermal differentiation in the inner parts of the differentiated 3D iPSC colonies (Figs. S3C–F, Fig. S4). The universal applicability of the nanofiber-microwell system to form a 3D stem cell colony and its patterned differentiation was confirmed by an embryonic stem cell line, H9 ESCs (Fig. S5). It should be noted that such a spatially organized multi-lineage differentiation pattern was only observed in the 3D colonies while PSCs cultured in 2D regular tissue culture plates differentiated only toward the mesendodermal lineage under the BMP4 stimulation (Fig. S6A).

Since both RhoA activity and mesodermal differentiation were observed at the outermost layers of the 3D iPSC colony, we examined whether this heterogeneity of differentiation behavior was regulated by the RhoA/ROCK signaling. ROCK activator, calpeptin, was simultaneously applied to the 3D iPSC colonies that were being subjected to the BMP4-induced differentiation. As shown in the confocal images (Fig. 2H, I, Figs. S6B and C), the application of the ROCK activator induced a more uniform distribution of T^+ cells in the inner parts of 3D iPSC colonies while those cells were localized only at the outermost layers in the absence of the ROCK activator. The increase in the number of cells differentiated to the mesendodermal lineage throughout the entire colony with ROCK activation indicates that ROCK activity during the formation of the 3D colony predisposes the cells to differentiate toward mesendodermal lineage under BMP4 stimulation (Fig. 2J). In fact, when iPSCs express active RhoA throughout the entire colony under 2D culture conditions (Fig. S2D), all cells differentiate only towards the mesendodermal lineage (Fig. S6A).

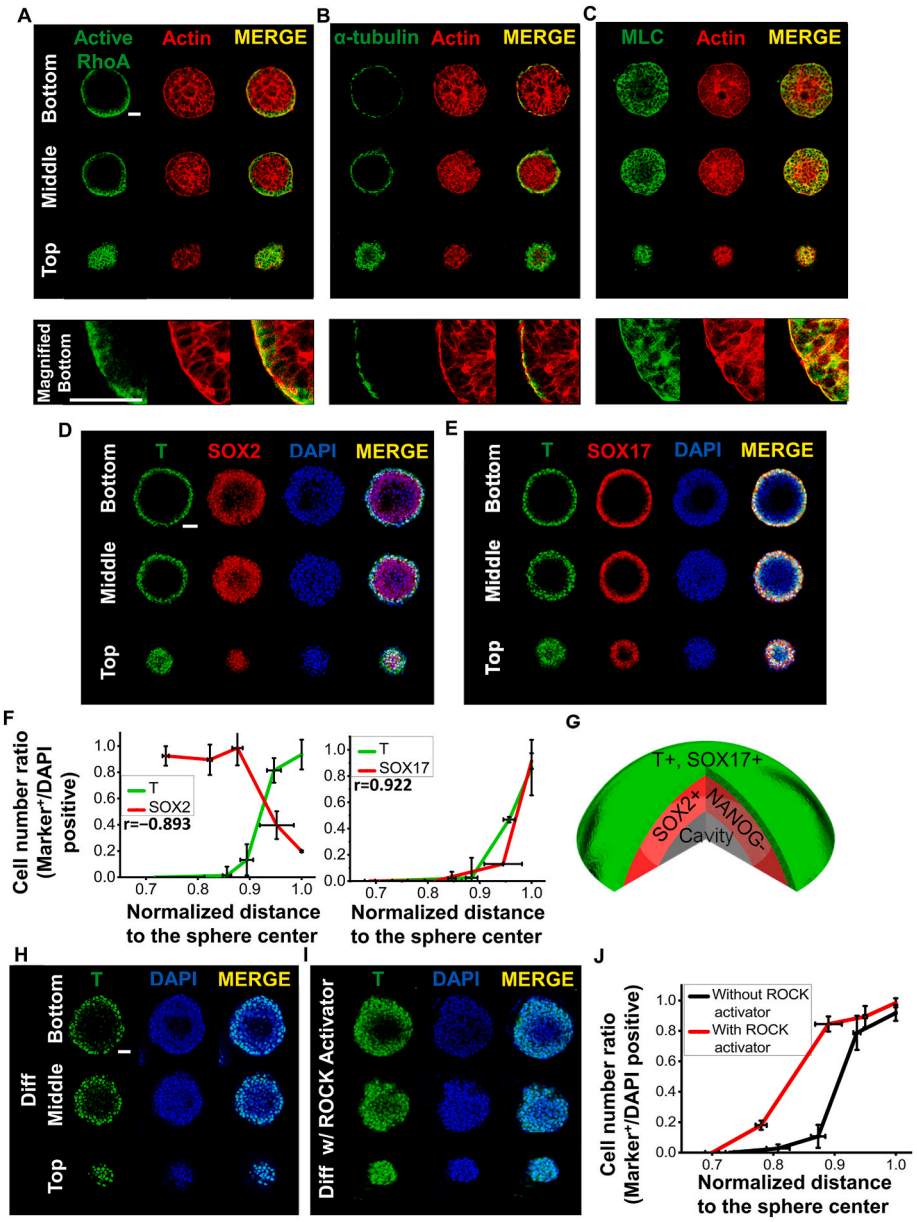

Fig. 2. 3D iPSC colonies in the microwell cell culture system exhibit a spatially patterned cytoskeletal organization and subsequent germ layer differentiation. (A) Representative confocal images of active RhoA expression at different z-sections showing localized RhoA activity in the outermost layers of the 3D iPSC colonies under the Prediff condition. (B, C) Representative confocal images of iPSC colonies showing the expression of (B) microtubule subunit α-tubulin or (C) non-muscle myosin light chain (MLC) and actin. Three representative cross-sectional images at the bottom (near the cell colony-substrate interface), middle, and top of the iPSC colonies are shown. (D, E) Confocal images of mesendodermal marker T and SOX17, ectodermal marker SOX2, expression within the 3D iPSC colonies under the Diff condition. Three representative cross-sectional images at the bottom (near the cell colony-substrate interface), middle, and top of the iPSC colonies are shown. (F) Quantification of lineage marker expression showing the 3D radial distribution of mesendodermal and ectodermal differentiation. Pearson's correlation coefficient (r) between the localization of T and SOX2 or T and SOX17 is noted. (G) Schematic of 3D radial distribution of cell lineages within the 3D hemispherical cell colony under the Diff condition. (H, I) Confocal images of T expression within 3D iPSC colonies without or with ROCK activator under the Diff condition. Three representative cross-sectional images at the bottom (near the cell colony-substrate interface), middle, and top of the iPSC colonies are shown. (J) Quantification of the expression data showing the 3D radial distribution of T^+ cells within the 3D iPSC colony without or with the application of ROCK activator. All scale bars = 50 μm.

3.3. YAP mediates mechanical microenvironment-induced spatially patterned germ layer differentiation

Epigenetic regulations have been shown to play key roles in mammalian development and lineage specification [37,38]. To explore the broad implication of epigenetic regulations during the formation of 3D iPSC colonies for the subsequent patterned differentiation, RNA sequencing was performed. A set of genes associated with epigenetics [18] was screened for comparison between the cells in the 3D iPSC colonies (Prediff) and those control cells grown as a monolayer in regular tissue culture plates (CTRL). The differential expression of the epigenetic-related genes showed that 981 genes had greater expression in Prediff while 1416 genes exhibited downregulation (Fig. 3A). The Gene Ontology (GO) enrichment analysis showed that the topmost enriched biological process among the epigenetics-related processes was demethylation (Fig. 3B). Similarly, protein demethylation and histone demethylation were positioned within the top 5 most enriched biological processes, while the formation of the primary germ layer and mesoderm development were also highly enriched along with the demethylation processes (Fig. 3B). Based on this observation, detailed

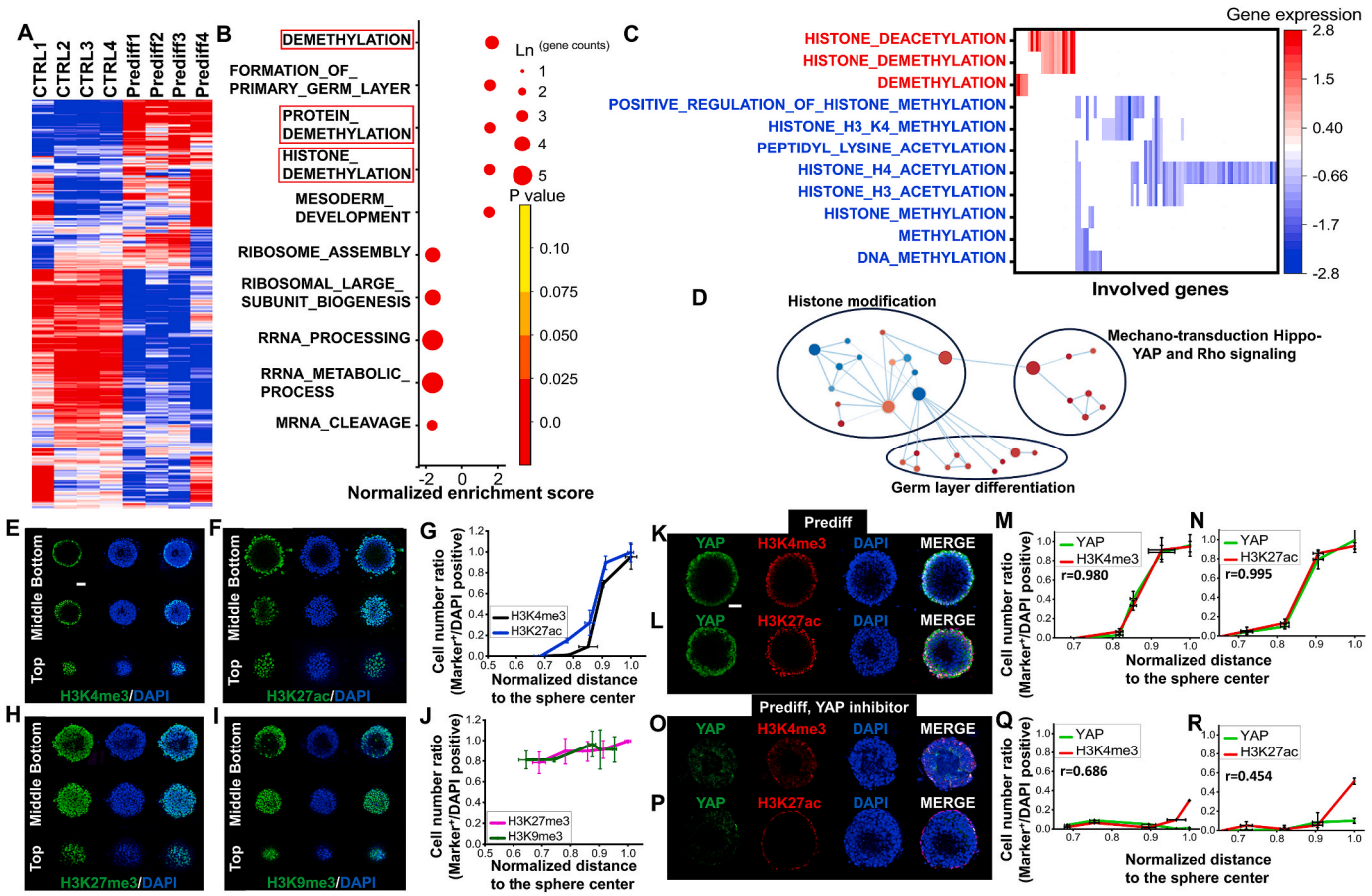

Fig. 3. YAP mediates mechanical microenvironment-induced spatially patterned germ layer differentiation. (A) A hierarchically clustered heatmap showing the expression patterns of all epigenetic-related genes. Red and blue represent the upregulation and downregulation of genes under the Prediff condition, as compared to the control (CTRL) group where iPSCs were cultured in tissue culture plates as 2D monolayers. (B) A GO enrichment analysis of biological processes between the CTRL and the Prediff conditions. The circle size indicates the natural logarithm of the gene counts of each biological process. The circle color indicates the significance of the normalized enrichment score of each biological process. (C) Gene expression heatmap of GO enrichment analysis showing the difference in epigenetic regulation of the Prediff condition, as compared to the CTRL group. (D) Node network analysis of signaling pathways involving mechano-transduction Hippo-YAP and Rho signaling, histone modification, and germ layer differentiation. The number of genes in each GO is displayed as node size. Blue nodes indicate downregulated biological processes while red nodes indicate upregulated biological processes under the Prediff condition. Nodes were manually laid out to form a clearer picture while clusters of nodes were labeled using the AutoAnnotate plugin within the Cytoscape software. (E, F, H, I) Confocal images showing the expression of histone modification markers (E) H3K4me3, (F) H3K27ac, (H) H3K27me3, and (I) H3K9me3 within 3D iPSC colonies under the Prediff condition. (G, J) Corresponding quantification of histone modification expression, showing the radial distribution of each histone modification marker within the cell colonies. (K, L) Representative confocal images showing the expression of (K) YAP and H3K4me3, or (L) H3K27ac in 3D iPSC colonies under the Prediff condition. (M, N) Distribution quantification of (M) YAP and H3K4me3-positive cells, or (N) YAP, H3K27ac-positive cells within the 3D iPSC colonies under the Prediff condition (n = 3). Pearson's correlation coefficient (r) between YAP and H3K4me3 or YAP and H3K27ac is noted. (O, P) Representative confocal images showing the expression of (O) YAP and H3K4me3, or (P) H3K27ac in 3D iPSC colonies under Prediff condition with the application of YAP inhibitor. (Q, R) Distribution quantification of (Q) YAP and H3K4me3-positive cells, or (R) YAP, H3K27ac-positive cells within the 3D iPSC colonies under the Prediff condition with the application of YAP inhibitor (n = 3). Pearson's correlation coefficient (r) between YAP and H3K4me3 or YAP and H3K27ac is noted. All scale bars = 50 μm. (For interpretation of the references to color in this figure legend, the reader is referred to the Web version of this article.)

GO-enriched biological processes including broader aspects of protein histone modifications were plotted as a heatmap, showing a clear trend that histone demethylation and deacetylation processes were upregulated under the Prediff condition while the histone methylation and acetylation processes were downregulated (Fig. 3C). Furthermore, a pathway analysis tool (Cytoscape) was utilized to generate a transcriptome-based gene regulatory network (Fig. 3D), where the associated biological processes were labeled (Fig. S7). A clearly observed interconnection among mechanotransduction signaling (including Hippo-YAP and Rho), histone modifications, and iPSC germ layer differentiation, suggests the involvement of histone modifications in the mechano-modulated germ layer specification within the 3D iPSC colonies.

To visualize the epigenetic states of the cells, we utilized immunostaining which enables the capture of heterogeneously changing overall histone modification levels within the 3D iPSC colonies [39,40]. Confocal imaging showed that the histone modification markers of transcriptional activators including trimethylation of histone H3 at lysine 4 (H3K4me3), acetylation of histone H3 at lysine 27 (H3K27ac) remained active only at the outermost layers of the colonies after forming 3D colonies (Fig. 3E–G, Figs. S8A and B) as compared to the uniform expression of those epigenetic markers in the cells cultured in regular tissue culture plates to form 2D colonies (Figs. S8C and D). In contrast, gene repressors including trimethylation of histone 3 at lysine 27 (H3K27me3) and trimethylation of histone 3 at lysine 9 (H3K9me3), were more uniformly distributed within Prediff 3D iPSC colonies (Fig. 3H–J, Figs. S8E and F). These results suggest that the activators of histone modification (H3K4me3 and H3K27ac) are potentially mechano-responsive and regulated by the spatially varied mechanical cues within the 3D iPSC colonies since these histone modification

markers and mechano-sensitive RhoA share a similar expression pattern (Fig. 2A and 3E, F). Therefore, considering the RNA sequencing results (Fig. 3B and C), we showed that the upregulation of demethylation and deacetylation (or the loss of H3K4me3 and H3K27ac expression as compared to the control) occurs in the inner parts of the 3D colony while the peripheral areas maintain the histone modification (Fig. 3E and F).

To confirm the mechano-sensitivity of the histone modification of gene activators, we next examined the relationship between histone modification and YAP, which has been shown to play a crucial role in cellular mechanotransduction [41] and was found to be important for the epigenetic regulation of iPSC differentiation according to the nodal network analysis (Fig. 3D, Fig. S7). While the expression patterns of YAP and H3K4me3/H3K27ac were uniformly expressed in 2D monolayer iPSCs cultured on regular tissue culture plates (Figs. S8C and D), they were localized in a confined region only at the outermost layers within 3D iPSC colonies (Fig. 3K-N, Figs. S9A and B). The application of a YAP inhibitor, verteporfin, induced the loss of YAP and H3K4me3/H3K27ac expression almost throughout the entire colonies, indicating that YAP

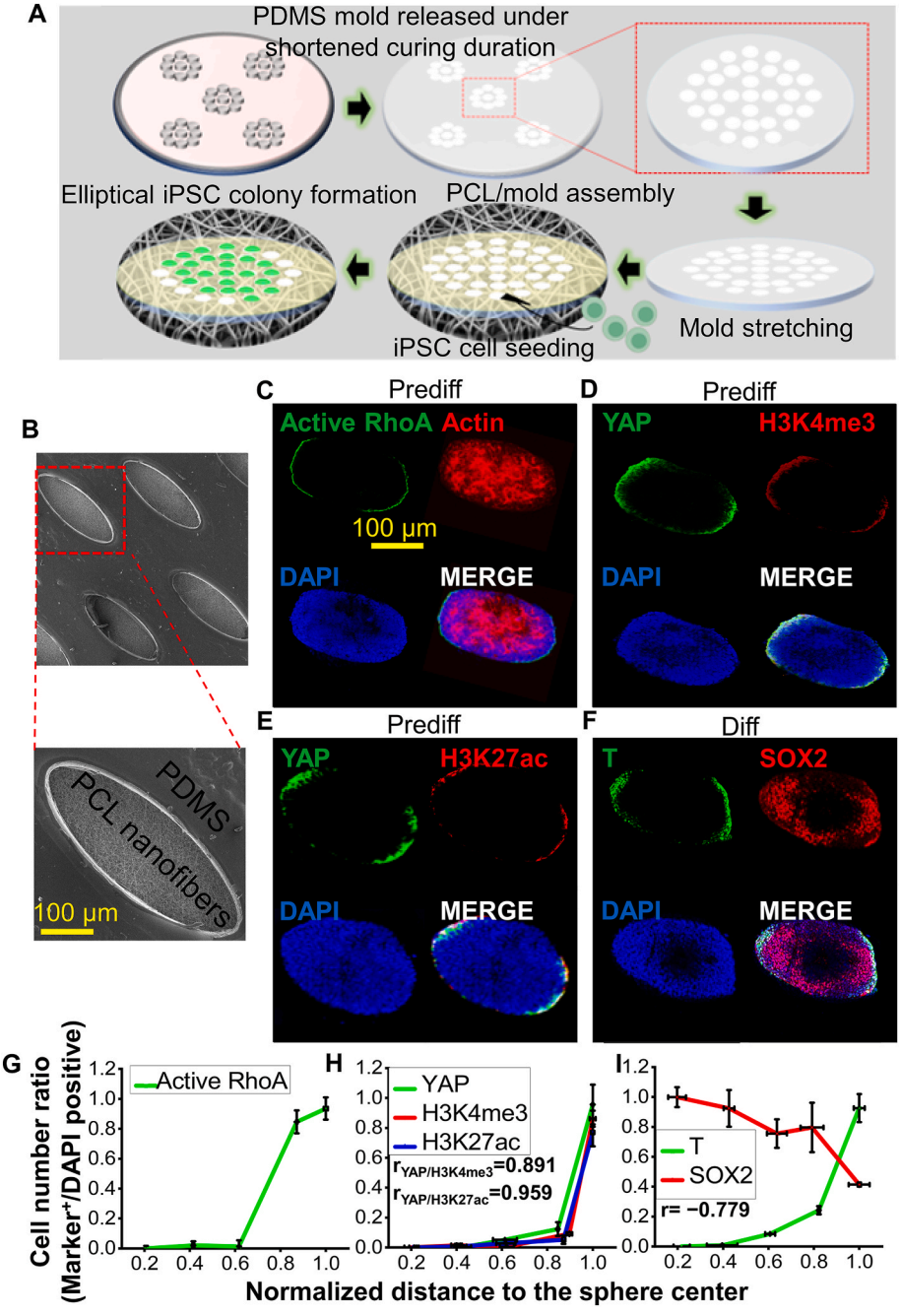

Fig. 4. Spatially organized differentiation pattern is regulated by the 3D form of iPSC colonies via control over the shape of the nanofiber microwells. (A) A schematic showing the fabrication process of the nanofiber-microwell cell culture system with elongated microwells. (B) SEM images showing the elliptical morphology of PDMS microwells attached to PCL nanofibers to physically control the morphology of 3D iPSC colonies. (C–F) Localized expression of various mechano-sensitive, histone modification, or differentiation markers including (C) active RhoA and actin, (D) YAP and H3K4me3, (E) YAP and H3K27ac, and (F) T and SOX2. Mechano-sensitive markers (active RhoA and YAP) and histone modification markers (H3K4me3 and H3K27ac) were examined after 5 days of preculture while differentiation markers (T and SOX2) were observed in the iPSC colonies which were subjected to subsequent BMP4 stimulation for 36 h. (G–I) The corresponding quantification shows the localized expression of various markers at the vertices within the elliptical cell colonies (n = 3). Pearson's correlation coefficient (r) between YAP and H3K4me3, YAP and H3K27ac, or T and SOX2 is noted.

signaling regulates the activators of histone modification (Fig. 3O-R, Figs. S9C and D). In contrast, there was little or no change in the expression pattern of gene repressors after the YAP inhibitor application, as compared to that under the Prediff condition (Fig. 3H, I, Figs. S10A–C). Collectively, these results demonstrate that the spatially organized heterogeneity of histone modification of gene activators is mediated by YAP signaling, aligned with other studies where YAP-regulated activity of H3K4me3 or H3K27ac, and YAP-independent activity of H3K27me3 or H3K9me3 have been observed [42–44]. Furthermore, a YAP activator, PY60, was used to examine if there is any regulatory correlation between patterned YAP expression under the Prediff condition and patterned germ layer expression under the Diff condition. It was observed that mesendodermal marker T was expressed substantially more inside the colony, similar to that observed under the application of the ROCK activator (Fig. 2I), demonstrating the regulatory role of YAP in germ layer differentiation (Figs. S11A and B).

3.4. Spatially organized differentiation pattern is regulated by the 3D form of iPSC colonies via control over the shape of the microwells

The presented results have collectively shown a spatial regulation of iPSC differentiation, mediated through the mechano-sensitive and histone modification signaling pathways, where cells experience greater stresses at the outermost layers of the 3D colonies as compared to the cells that were located in the inner parts. To further confirm whether this patterned, heterogeneous differentiation was indeed controlled by the mechanical microenvironment, we modified our cell culture system utilizing a PDMS mold having an anisotropic microwell shape to control the morphology of iPSC colonies (Fig. 4A and B). Due to physical restriction, iPSCs grown in this modified microwell culture system formed elliptical-shaped colonies. In comparison to the hemispherical iPSC colonies where active RhoA and YAP were expressed at the entire outermost layers (Fig. 2A and 3K), these two mechano-mediators were only expressed at both vertices of the elliptical colonies (Fig. 4C, D, G, H). Following such an expression pattern of mechano-mediators within the elliptical colonies, histone modification markers, H3K4me3 and H3K27ac, were also localized at the two vertices (Fig. 4D, E, H). Furthermore, the location-dependent heterogeneous differentiation matched the expression pattern of these mechano-mediators and histone modification markers, where mesendodermal marker T was localized at the elliptical vertices (Fig. 4F–I). The ectodermal marker, SOX2, on the other hand, was expressed in the areas where active RhoA and YAP expressions were absent in the inner region and long edge of the elliptical colonies. Note that there were no significant volume differences between the hemispherical and elliptical iPSC colonies, indicating that the difference in differentiation pattern between hemispherical and elliptical colonies is not due to different cell densities (Figs. S12A and B). In addition, NANOG was uniformly expressed throughout the entire colonies for both the hemispherical and elliptical shapes (Figs. S13A and B), demonstrating that little or no effect of colony shape on maintaining the stemness of the iPSC colonies before being subjected to differentiation.

4. Discussion

In this study, a cell culture system, composed of an electrospun PCL nanofibrous substrate and PDMS microwells, was engineered to control the formation of 3D iPSC colonies. With the restrained cell culture space (within the microwells), 3D iPSC colony morphologies were controlled to be hemispherical with the spatially patterned mechanical microenvironment. Microwell culture plates are commercially available for small-sized 3D cell colony culture. These microplates, however, are typically used for suspension culture or the formation of the embryonic body. Our microwell culture system, on the other hand, provides a platform to form 3D hemispherical colonies with the bottom colony surface attached to the substrate, providing a stable substrate to immobilize the cells, resulting in a more controlled cellular environment. In addition, commercially available microwell plates only provide limited sizes and shapes while our microwell system enables the tuning of both parameters depending on specific applications. In the 3D iPSC colonies induced by the nanofiber-microwell culture system, heterogeneous differentiation (inner parts: ectodermal differentiation, outermost layer: mesendodermal differentiation) was observed when the cells were exposed to BMP4, which is frequently used for the induction of multilineage differentiation of iPSCs [12,35]. Although a radial pattern can also be developed from 2D iPSC monolayers [10,12,45], their mechanical environments are significantly different; greater cell-substrate traction forces on the edges lead to the activation of mechano-signaling in the 2D models while cell-cell interaction mediates the patterned differentiation of the 3D hemispherical colonies. Within the 3D hemispherical colonies, a similar pattern was observed in the expression of mechano-sensitive mediators and cytoskeleton; the data showed that the activity of RhoA is highly localized to the area of high tension, i.e., the outermost layers of the 3D hemispherical colony, resulting in the development of actomyosin cables. This heterogeneous mechanical microenvironment was further confirmed by the cytoskeleton component expression within the 3D iPSC colonies, where highly organized cytoskeleton structure, including the localized α-tubulin expression as well as the strong actin-myosin interactions, were observed at the outermost layers of the 3D iPSC colonies. These results collectively demonstrate that cells localized at the higher tension area (outermost layer) within the 3D colony differentiated towards mesendodermal lineage while cells at the lower tension area (inner layer) differentiated towards ectodermal lineage. This mechanical environment-specific differentiation pattern was consistent with a previous study demonstrating tension-dependent mesoderm differentiation [46].

In conjunction with this patterned differentiation, we investigated how chromatin histone modification is regulated in 3D iPSC colonies as compared to 2D iPSC monolayers. The GO enrichment analysis indicated that histone demethylation and deacetylation were upregulated in 3D iPSC colonies, likely in the cells in the inner parts of the colonies based on the imaging data. More interestingly, we revealed that the histone modification of gene activators (H3K4me3 and H3K27ac) under the Prediff condition showed a similar pattern to the differentiation markers T and SOX17 under the Diff condition, also localized to the outermost layers of the 3D colony, where weak or no expression of H3K4me3, H3K27ac under the Prediff condition were observed in the inner parts of the 3D iPSC colonies. Moreover, the effect of a mechano-mediator YAP on histone modification and subsequent germ layer differentiation was examined since a correlation between Hippo-YAP signaling and histone modifications was observed from the network analysis of the biological processes. The spatially localized YAP expression under the Prediff condition as well as the deactivation of the histone modification of gene activators after the YAP inhibition suggest a strong regulatory effect of YAP on the histone modification. These results are consistent with the previous studies showing active roles of YAP in gene regulation with various mechanisms. Examples include the YAP/TAZ complex and its coactivator BRD4 exhibit binding sites exclusively towards activators [47]. More specifically, studies have identified a subunit of gene activator H3K4 methyltransferase complex called Ncoa6, as an active binding site of YAP, resulting in the activation of H3K4 activator [42]. Moreover, evidence revealed that YAP recruits its coactivator, p300, which binds and acetylated sites of H3K27ac, resulting in the activation of the H3K27 activators [42]. On the other hand, corroborating with our results, several studies have shown that there is little or no effect of YAP on gene repressors such as H3K27me3 and H3K9me3 [43,44]. Interestingly, YAP nuclear localization was observed under the Prediff condition while YAP cytoplasmic translocation occurred under the Diff condition (Fig. S14), suggesting diverse roles of YAP in maintaining pluripotency as well as inducing differentiation [48].

Previous studies have shown that RhoA/ROCK acts upstream of YAP

in the mechano-transduction signaling [49,50]. Therefore, this work highlights the use of the engineered nanofiber-microwell cell culture system in regulating iPSC germ layer differentiation in 3D, through the control of mechanical microenvironment and subsequent mechano-sensing mediators as well as histone modifications. Note that a similar histone modification pattern has also been observed by other researchers where the increase in the overall levels of histone modification H3K4me3 and H3K27ac was accompanied by mesendodermal differentiation [51,52]. However, despite a link between histone modification and germ layer differentiation was observed, the investigation of histone modification in response to cellular mechano-transduction behavior in our study is limited to overall histone modification levels while how such localized changes in histone modification directly affect specific gene expression, thus differentiation remains unknown. Therefore, follow-up studies are to be conducted to explore the effects of mechanotransduction on a broader aspect of epigenetic regulation on specific gene expression/repression in a spatially resolved manner.

Nevertheless, elliptical iPSC colonies were engineered to further confirm the RhoA/ROCK-YAP-histone modification signaling axis for the potential regulation of iPSC differentiation. Unlike mesendodermal differentiation localized at the entire circumference of the outermost layer in the hemispherical iPSC colonies, elliptical colonies showed mesendodermal differentiation only at the two vertices of the ellipse. Such differences in the differentiation pattern were likely attributed to different cellular mechanical environments between hemispherical and elliptical colonies. As shown by others [46,53–55], cells located at the outer edge of a circular colony experience a relatively similar high traction stress while cells located at the two vertices of the elliptical colony experience greater stress as compared to the cell in the long edges. Such a cellular stress distribution, which coincides with the spatial activation of the mechano-mediators examined in this study, further supports our hypothesis that control over colony morphology regulates mechano-transduction signaling pathways, modulating the downstream histone modification and subsequent germ layer differentiation. This emphasizes the potential of the nanofiber-microwell cell culture system for developing in vitro 3D stem cell models, enabling the studies of heterogenous mechanical microenvironment-modulated germ layer differentiation, and gaining insights into mechano-transduction mechanisms of 3D iPSC colonies.

Different from 3D gastruloids, the microwell system developed in this study enables a controllable hemispherical shape and consistent colony size while typical 3D gastruloids exhibit various shapes and sizes [56,57]. Such consistency within the nanofiber-microwell system in terms of colony size and differentiation behavior enables us to gain robust insight into the role of signaling pathways in the organization of early germ layer fate. This study did not intend to replicate the gastrulation process during embryonic development, which even the most recent gastruloid model cannot precisely depict [58,59]. Collectively, the results emphasize the potential of the nanofiber-microwell cell culture system for developing in vitro 3D stem cell models, studying the heterogenous mechanical microenvironment-affected germ layer differentiation, and investigating the mechanisms of the spatially patterned cellular behavior.

5. Conclusion

This study presents a novel stem cell culture system engineered to precisely control spatial differentiation patterns in iPSC colonies through manipulation of their 3D morphology and, consequently, their mechanical microenvironment. We demonstrate that RhoA activity exhibits localized spatial organization within the colony, driving downstream YAP activation, chromatin remodeling, and lineage specification. Notably, we effectively modulated the mechanical microenvironment by controlling the shape of stem cell colonies, leading to a spatial change of mechano-mediator activation from the entire outermost layers of the hemispherical colonies to only the vertices of the elliptical colonies. Correspondingly, specific histone modifications as well as subsequent mesendodermal differentiation followed a similar spatial pattern, suggesting the RhoA/ROCK-YAP-histone modification signaling axis for the potential regulation of iPSC differentiation.

CRediT authorship contribution statement

Youyi Tai: Writing – review & editing, Writing – original draft, Methodology, Investigation, Formal analysis, Data curation. **Robyn Goodrich:** Writing – original draft, Visualization, Methodology, Formal analysis, Data curation. **Maricela Maldonado:** Writing – review & editing, Writing – original draft, Investigation, Formal analysis, Data curation, Conceptualization. **Jessica Ortiz:** Writing – review & editing, Methodology, Investigation, Formal analysis, Data curation. **Jeniree Martinez:** Writing – review & editing, Methodology, Investigation, Formal analysis, Data curation. **Gerardo Ico:** Writing – review & editing, Methodology, Investigation, Formal analysis, Data curation. **Angel Ko:** Writing – review & editing, Methodology, Investigation, Formal analysis, Data curation. **Hung Ping Shih:** Writing – review & editing, Writing – original draft, Supervision, Project administration, Funding acquisition, Formal analysis, Data curation, Conceptualization. **Jin Nam:** Writing – review & editing, Writing – original draft, Visualization, Validation, Supervision, Resources, Project administration, Investigation, Funding acquisition, Formal analysis, Data curation, Conceptualization.

Declaration of competing interest

The authors declare the following financial interests/personal relationships which may be considered as potential competing interests: Jin Nam reports financial support was provided by UC-KIMS center for innovative materials. Hung-Ping Shih reports financial support was provided by Wanek Family Foundation to Cure Type 1 Diabetes. Hung-Ping Shih reports financial support was provided by National Institute of Health. Youyi Tai reports financial support was provided by California Institute for Regenerative Medicine. If there are other authors, they declare that they have no known competing financial interests or personal relationships that could have appeared to influence the work reported in this paper.

Data availability

Data will be made available on request.

Acknowledgements

This work was supported by UC Riverside and Korea Institute of Materials Science through UC-KIMS Center for Innovative Materials for Energy and Environment (Research Program PNK7280 (Nam)), Wanek Family Foundation to Cure Type 1 Diabetes (Shih), and NIH/NIDDK (R01DK119590 (Shih)). Y.T. was supported by a TRANSCEND fellowship from the California Institute for Regenerative Medicine (EDUC4-12752). The contents of this publication are solely the responsibility of the authors and do not necessarily represent the official view of CIRM or other agencies of the State of California.

Appendix A. Supplementary data

Supplementary data to this article can be found online at https://doi.org/10.1016/j.mtbio.2024.101109.

References

[1] K. Takahashi, S. Yamanaka, Induction of pluripotent stem cells from mouse embryonic and adult fibroblast cultures by defined factors, Cell 126 (4) (2006) 663–676, https://doi.org/10.1016/j.cell.2006.07.024.

[2] Y. Zhao, X.L. Yin, H. Qin, F.F. Zhu, H.S. Liu, W.F. Yang, Q. Zhang, C.A. Xiang, P. P. Hou, Z.H. Song, Y.X. Liu, J. Yong, P.B. Zhang, J. Cai, M. Liu, H.G. Li, Y.Q. Li, X. X. Qu, K. Cui, W.Q. Zhang, T.T. Xiang, Y.T. Wu, Y.D. Zhao, C. Liu, C. Yu, K.H. Yuan, J.N. Lou, M.X. Ding, H.K. Deng, Two supporting factors greatly improve the efficiency of human iPSC generation, Cell Stem Cell 3 (5) (2008) 475–479, https://doi.org/10.1016/j.stem.2008.10.002.

[3] M. Maldonado, R.J. Luu, G. Ico, A. Ospina, D. Myung, H.P. Shih, J. Nam, Lineage- and developmental stage-specific mechanomodulation of induced pluripotent stem cell differentiation, Stem Cell Res. Ther. 8 (1) (2017) 216, https://doi.org/10.1186/s13287-017-0667-2.

[4] H.P. Bei, P.M. Hung, H.L. Yeung, S. Wang, X. Zhao, Bone-a-Petite: engineering exosomes towards bone, osteochondral, and cartilage repair, Small 17 (50) (2021) e2101741, https://doi.org/10.1002/smll.202101741.

[5] J.A. Rivera-Perez, A.K. Hadjantonakis, The dynamics of morphogenesis in the early mouse embryo, Cold Spring Harbor Perspect. Biol. 7 (11) (2014), https://doi.org/10.1101/cshperspect.a015867.

[6] M. Simunovic, J.J. Metzger, F. Etoc, A. Yoney, A. Ruzo, I. Martyn, G. Croft, D. S. You, A.H. Brivanlou, E.D. Siggia, A 3D model of a human epiblast reveals BMP4-driven symmetry breaking, Nat. Cell Biol. 21 (7) (2019) 900–910, https://doi.org/10.1038/s41556-019-0349-7.

[7] J. Li, Y. Liu, Y. Zhang, B. YaoEnhejirigala, Z. Li, W. Song, Y. Wang, X. Duan, X. Yuan, X. Fu, S. Huang, Biophysical and biochemical cues of biomaterials guide mesenchymal stem cell behaviors, Front. Cell Dev. Biol. 9 (2021) 640388, https://doi.org/10.3389/fcell.2021.640388.

[8] K.H. Vining, D.J. Mooney, Mechanical forces direct stem cell behaviour in development and regeneration, Nat. Rev. Mol. Cell Biol. 18 (12) (2017) 728–742, https://doi.org/10.1038/nrm.2017.108.

[9] G. Abagnale, A. Sechi, M. Steger, Q. Zhou, C.C. Kuo, G. Aydin, C. Schalla, G. Muller-Newen, M. Zenke, I.G. Costa, P. van Rijn, A. Gillner, W. Wagner, Surface topography guides morphology and spatial patterning of induced pluripotent stem cell colonies, Stem Cell Rep. 9 (2) (2017) 654–666, https://doi.org/10.1016/j.stemcr.2017.06.016.

[10] K.T. Minn, Y.H.C. Fu, S.H. He, S. Dietmann, S.C. George, M.A. Anastasio, S. A. Morris, L. Solnica-Krezel, High-resolution transcriptional and morphogenetic profiling of cells from micropatterned human ESC gastruloid cultures, Elife 9 (2020) e59445, https://doi.org/10.7554/eLife.59445.

[11] A. Vickers, M. Tewary, A. Laddach, M. Poletti, V. Salameti, F. Fraternali, D. Danovi, F.M. Watt, Plating human iPSC lines on micropatterned substrates reveals role for ITGB1 nsSNV in endoderm formation, Stem Cell Rep. 16 (11) (2021) 2628–2641, https://doi.org/10.1016/j.stemcr.2021.09.017.

[12] A. Warmflash, B. Sorre, F. Etoc, E.D. Siggia, A.H. Brivanlou, A method to recapitulate early embryonic spatial patterning in human embryonic stem cells, Nat. Methods 11 (8) (2014) 847–854, https://doi.org/10.1038/Nmeth.3016.

[13] S. Scuderi, G.G. Altobelli, V. Cimini, G. Coppola, F.M. Vaccarino, Cell-to-Cell adhesion and neurogenesis in human cortical development: a study comparing 2D monolayers with 3D organoid cultures, Stem Cell Rep. 16 (2) (2021) 264–280, https://doi.org/10.1016/j.stemcr.2020.12.019.

[14] M. Maldonado, L.Y. Wong, C. Echeverria, G. Ico, K. Low, T. Fujimoto, J.K. Johnson, J. Nam, The effects of electrospun substrate-mediated cell colony morphology on the self-renewal of human induced pluripotent stem cells, Biomaterials 50 (2015) 10–19, https://doi.org/10.1016/j.biomaterials.2015.01.037.

[15] A.M. Bolger, M. Lohse, B. Usadel, Trimmomatic: a flexible trimmer for Illumina sequence data, Bioinformatics 30 (15) (2014) 2114–2120, https://doi.org/10.1093/bioinformatics/btu170.

[16] S. Chen, Y. Zhou, Y. Chen, J. Gu, fastp: an ultra-fast all-in-one FASTQ preprocessor, Bioinformatics 34 (17) (2018) i884–i890, https://doi.org/10.1093/bioinformatics/bty560.

[17] A. Dobin, C.A. Davis, F. Schlesinger, J. Drenkow, C. Zaleski, S. Jha, P. Batut, M. Chaisson, T.R. Gingeras, STAR: ultrafast universal RNA-seq aligner, Bioinformatics 29 (1) (2013) 15–21, https://doi.org/10.1093/bioinformatics/bts635.

[18] M. Lu, S. Qiu, X. Jiang, D. Wen, R. Zhang, Z. Liu, Development and validation of epigenetic modification-related signals for the diagnosis and prognosis of hepatocellular carcinoma, Front. Oncol. 11 (2021) 649093, https://doi.org/10.3389/fonc.2021.649093.

[19] V.K. Mootha, C.M. Lindgren, K.F. Eriksson, A. Subramanian, S. Sihag, J. Lehar, P. Puigserver, E. Carlsson, M. Ridderstrale, E. Laurila, N. Houstis, M.J. Daly, N. Patterson, J.P. Mesirov, T.R. Golub, P. Tamayo, B. Spiegelman, E.S. Lander, J. N. Hirschhorn, D. Altshuler, L.C. Groop, PGC-1alpha-responsive genes involved in oxidative phosphorylation are coordinately downregulated in human diabetes, Nat. Genet. 34 (3) (2003) 267–273, https://doi.org/10.1038/ng1180.

[20] A. Subramanian, P. Tamayo, V.K. Mootha, S. Mukherjee, B.L. Ebert, M.A. Gillette, A. Paulovich, S.L. Pomeroy, T.R. Golub, E.S. Lander, J.P. Mesirov, Gene set enrichment analysis: a knowledge-based approach for interpreting genome-wide expression profiles, Proc. Natl. Acad. Sci. U.S.A. 102 (43) (2005) 15545–15550, https://doi.org/10.1073/pnas.0506580102.

[21] C.N. Yau, H.M. Lai, K. Lee, A.J. Kwok, J. Huang, H. Ko, Principles of deep immunohistochemistry for 3D histology, Cell Rep Methods 3 (5) (2023) 100458, https://doi.org/10.1016/j.crmeth.2023.100458.

[22] E.C. Costa, D.N. Silva, A.F. Moreira, I.J. Correia, Optical clearing methods: an overview of the techniques used for the imaging of 3D spheroids, Biotechnol. Bioeng. 116 (10) (2019) 2742–2763, https://doi.org/10.1002/bit.27105.

[23] H.J. Schunemann, L. Griffith, R. Jaeschke, R. Goldstein, D. Stubbing, G.H. Guyatt, Evaluation of the minimal important difference for the feeling thermometer and the St. George's Respiratory Questionnaire in patients with chronic airflow obstruction, J. Clin. Epidemiol. 56 (12) (2003) 1170–1176, https://doi.org/10.1016/s0895-4356(03)00115-x.

[24] S. Williams, Pearson's correlation coefficient, N. Z.Med. J. 109 (1015) (1996) 38.

[25] M. Pajic, D. Herrmann, C. Vennin, J.R. Conway, V.T. Chin, A.K. Johnsson, H. C. Welch, P. Timpson, The dynamics of Rho GTPase signaling and implications for targeting cancer and the tumor microenvironment, Small GTPases 6 (2) (2015) 123–133, https://doi.org/10.4161/21541248.2014.973749.

[26] T. Zhang, T. Gong, J. Xie, S. Lin, Y. Liu, T. Zhou, Y. Lin, Softening substrates promote chondrocytes phenotype via RhoA/ROCK pathway, ACS Appl. Mater. Interfaces 8 (35) (2016) 22884–22891, https://doi.org/10.1021/acsami.6b07097.

[27] J. Chen, J. Irianto, S. Inamdar, P. Pravincumar, D.A. Lee, D.L. Bader, M.M. Knight, Cell mechanics, structure, and function are regulated by the stiffness of the three-dimensional microenvironment, Biophys. J. 103 (6) (2012) 1188–1197, https://doi.org/10.1016/j.bpj.2012.07.054.

[28] H. Gu, S.P. Yu, C.A. Gutekunst, R.E. Gross, L. Wei, Inhibition of the Rho signaling pathway improves neurite outgrowth and neuronal differentiation of mouse neural stem cells, Int J Physiol Pathophysiol Pharmacol 5 (1) (2013) 11–20.

[29] E. Maharam, M. Yaport, N.L. Villanueva, T. Akinyibi, D. Laudier, Z.Y. He, D. J. Leong, H.B. Sun, Rho/Rock signal transduction pathway is required for MSC tenogenic differentiation, Bone Res 3 (2015) 15015, https://doi.org/10.1038/boneres.2015.15.

[30] T.L. Chew, R.A. Masaracchia, Z.M. Goeckeler, R.B. Wysolmerski, Phosphorylation of non-muscle myosin II regulatory light chain by p21-activated kinase (gamma-PAK), J. Muscle Res. Cell Motil. 19 (8) (1998) 839–854, https://doi.org/10.1023/a:1005417926585.

[31] E. Kassianidou, J.H. Hughes, S. Kumar, Activation of ROCK and MLCK tunes regional stress fiber formation and mechanics via preferential myosin light chain phosphorylation, Mol. Biol. Cell 28 (26) (2017) 3832–3843, https://doi.org/10.1091/mbc.E17-06-0401.

[32] M. Brown, D. Adyshev, V. Bindokas, J. Moitra, J.G. Garcia, S.M. Dudek, Quantitative distribution and colocalization of non-muscle myosin light chain kinase isoforms and cortactin in human lung endothelium, Microvasc. Res. 80 (1) (2010) 75–88, https://doi.org/10.1016/j.mvr.2009.12.010.

[33] T. Kampourakis, Y.B. Sun, M. Irving, Myosin light chain phosphorylation enhances contraction of heart muscle via structural changes in both thick and thin filaments, P Natl Acad Sci USA 113 (21) (2016) E3039–E3047, https://doi.org/10.1073/pnas.1602776113.

[34] L.C. Boraas, E.T. Pineda, T. Ahsan, Actin and myosin II modulate differentiation of pluripotent stem cells, PLoS One 13 (4) (2018) e0195588, https://doi.org/10.1371/journal.pone.0195588.

[35] M. Maldonado, R.J. Luu, M.E. Ramos, J. Nam, ROCK inhibitor primes human induced pluripotent stem cells to selectively differentiate towards mesendodermal lineage via epithelial-mesenchymal transition-like modulation, Stem Cell Res. 17 (2) (2016) 222–227, https://doi.org/10.1016/j.scr.2016.07.009.

[36] L. Vallier, T. Touboul, Z. Chng, M. Brimpari, N. Hannan, E. Millan, L.E. Smithers, M. Trotter, P. Rugg-Gunn, A. Weber, R.A. Pedersen, Early cell fate decisions of human embryonic stem cells and mouse epiblast stem cells are controlled by the same signalling pathways, PLoS One 4 (6) (2009) e6082, https://doi.org/10.1371/journal.pone.0006082.

[37] S.J. Meng, H.C. Zhou, Z.Y. Feng, Z.H. Xu, Y. Tang, M.H. Wu, Epigenetics in neurodevelopment: emerging role of circular RNA, Front. Cell. Neurosci. 13 (2019) 327, https://doi.org/10.3389/fncel.2019.00327.

[38] R.M. Xu, C. Li, X.Y. Liu, S.R. Gao, Insights into epigenetic patterns in mammalian early embryos, Protein Cell 12 (1) (2021) 7–28, https://doi.org/10.1007/s13238-020-00757-z.

[39] T. Wongtawan, J.E. Taylor, K.A. Lawson, I. Wilmut, S. Pennings, Histone H4K20me3 and HP1alpha are late heterochromatin markers in development, but present in undifferentiated embryonic stem cells, J. Cell Sci. 124 (Pt 11) (2011) 1878–1890, https://doi.org/10.1242/jcs.080721.

[40] G. Sustackova, S. Legartova, S. Kozubek, L. Stixova, J. Pachernik, E. Bartova, Differentiation-independent fluctuation of pluripotency-related transcription factors and other epigenetic markers in embryonic stem cell colonies, Stem Cell. Dev. 21 (5) (2012) 710–720, https://doi.org/10.1089/scd.2011.0085.

[41] A. Elosegui-Artola, I. Andreu, A.E.M. Beedle, A. Lezamiz, M. Uroz, A.J. Kosmalska, R. Oria, J.Z. Kechagia, P. Rico-Lastres, A.L. Le Roux, C.M. Shanahan, X. Trepat, D. Navajas, S. Garcia-Manyes, P. Roca-Cusachs, Force triggers YAP nuclear entry by regulating transport across nuclear pores, Cell 171 (6) (2017) 1397–1410 e14, https://doi.org/10.1016/j.cell.2017.10.008.

[42] C. Stein, A.F. Bardet, G. Roma, S. Bergling, I. Clay, A. Ruchti, C. Agarinis, T. Schmelzle, T. Bouwmeester, D. Schubeler, A. Bauer, YAP1 exerts its transcriptional control via TEAD-mediated activation of enhancers, PLoS Genet. 11 (8) (2015) e1005465, https://doi.org/10.1371/journal.pgen.1005465.

[43] C. Estaras, H.T. Hsu, L. Huang, K.A. Jones, YAP repression of the WNT3 gene controls hESC differentiation along the cardiac mesoderm lineage, Genes Dev. 31 (22) (2017) 2250–2263, https://doi.org/10.1101/gad.307512.117.

[44] Y. Lu, T. Wu, O. Gutman, H. Lu, Q. Zhou, Y.I. Henis, K. Luo, Phase separation of TAZ compartmentalizes the transcription machinery to promote gene expression, Nat. Cell Biol. 22 (4) (2020) 453–464, https://doi.org/10.1038/s41556-020-0485-0.

[45] Y.C. Poh, J. Chen, Y. Hong, H. Yi, S. Zhang, J. Chen, D.C. Wu, L. Wang, Q. Jia, R. Singh, W. Yao, Y. Tan, A. Tajik, T.S. Tanaka, N. Wang, Generation of organized germ layers from a single mouse embryonic stem cell, Nat. Commun. 5 (2014) 4000, https://doi.org/10.1038/ncomms5000.

[46] J.M. Muncie, N.M.E. Ayad, J.N. Lakins, X. Xue, J. Fu, V.M. Weaver, Mechanical tension promotes formation of gastrulation-like nodes and patterns mesoderm specification in human embryonic stem cells, Dev. Cell 55 (6) (2020) 679–694 e11, https://doi.org/10.1016/j.devcel.2020.10.015.

[47] F. Zanconato, G. Battilana, M. Forcato, L. Filippi, L. Azzolin, A. Manfrin, E. Quaranta, D. Di Biagio, G. Sigismondo, V. Guzzardo, P. Lejeune, B. Haendler, J. Krijgsveld, M. Fassan, S. Bicciato, M. Cordenonsi, S. Piccolo, Transcriptional addiction in cancer cells is mediated by YAP/TAZ through BRD4, Nat. Med. 24 (10) (2018) 1599, https://doi.org/10.1038/s41591-018-0158-8.

[48] I. Lian, J. Kim, H. Okazawa, J. Zhao, B. Zhao, J. Yu, A. Chinnaiyan, M.A. Israel, L. S. Goldstein, R. Abujarour, S. Ding, K.L. Guan, The role of YAP transcription coactivator in regulating stem cell self-renewal and differentiation, Genes Dev. 24 (11) (2010) 1106–1118, https://doi.org/10.1101/gad.1903310.

[49] M. Ohgushi, M. Minaguchi, Y. Sasai, Rho-signaling-directed YAP/TAZ activity underlies the long-term survival and expansion of human embryonic stem cells, Cell Stem Cell 17 (4) (2015) 448–461, https://doi.org/10.1016/j.stem.2015.07.009.

[50] S. Dupont, L. Morsut, M. Aragona, E. Enzo, S. Giulitti, M. Cordenonsi, F. Zanconato, J. Le Digabel, M. Forcato, S. Bicciato, N. Elvassore, S. Piccolo, Role of YAP/TAZ in mechanotransduction, Nature 474 (7350) (2011) 179–183, https://doi.org/10.1038/nature10137.

[51] N.V. Bhanu, S. Sidoli, B.A. Garcia, Histone modification profiling reveals differential signatures associated with human embryonic stem cell self-renewal and differentiation, Proteomics 16 (3) (2016) 448–458, https://doi.org/10.1002/pmic.201500231.

[52] J.Y. Kim, H.M. Yang, J.E. Lee, M. Jeon, S.B. Bang, J. You, J. Kim, J. Lee, J. Hur, H. S. Kim, Enhanced generation of human induced pluripotent stem cells from peripheral blood and using their mesoderm differentiation ability to regenerate infarcted myocardium, Stem Cell. Int. 2022 (2022) 4104622, https://doi.org/10.1155/2022/4104622.

[53] E.N. Schaumann, M.F. Staddon, M.L. Gardel, S. Banerjee, Force localization modes in dynamic epithelial colonies, Mol. Biol. Cell 29 (23) (2018) 2835–2847, https://doi.org/10.1091/mbc.E18-05-0336.

[54] A.F. Mertz, S. Banerjee, Y. Che, G.K. German, Y. Xu, C. Hyland, M.C. Marchetti, V. Horsley, E.R. Dufresne, Scaling of traction forces with the size of cohesive cell colonies, Phys. Rev. Lett. 108 (19) (2012) 198101, https://doi.org/10.1103/PhysRevLett.108.198101.

[55] S.Z. Lin, B. Li, X.Q. Feng, A dynamic cellular vertex model of growing epithelial tissues, Acta Mech Sinica-Prc 33 (2) (2017) 250–259, https://doi.org/10.1007/s10409-017-0654-y.

[56] M. Merle, L. Friedman, C. Chureau, A. Shoushtarizadeh, T. Gregor, Precise and scalable self-organization in mammalian pseudo-embryos, Nat. Struct. Mol. Biol. (2024), https://doi.org/10.1038/s41594-024-01251-4.

[57] A.E. Sullivan, S.D. Santos, The ever-growing world of gastruloids: autogenous models of mammalian embryogenesis, Curr. Opin. Genet. Dev. 82 (2023) 102102, https://doi.org/10.1016/j.gde.2023.102102.

[58] S. Ghimire, V. Mantziou, N. Moris, A. Martinez Arias, Human gastrulation: the embryo and its models, Dev. Biol. 474 (2021) 100–108, https://doi.org/10.1016/j.ydbio.2021.01.006.

[59] S.C. van den Brink, A. van Oudenaarden, 3D gastruloids: a novel frontier in stem cell-based in vitro modeling of mammalian gastrulation, Trends Cell Biol. 31 (9) (2021) 747–759, https://doi.org/10.1016/j.tcb.2021.06.007.